Available online at www.sciencedirect.com
ScienceDirect
Trans. Nonferrous Met. Soc. China 31(2021) 11−23
Transactions of Nonferrous Metals Society of China
www.tnmsc.cn

Effect of alloying elements on thermal stability of nanocrystalline Al alloys

Hany Rizk AMMAR[1,2], Muneer BAIG[3], Asiful Hossain SEIKH[4], Jabair Ali MOHAMMED[4]

1. Mechanical Engineering Department, College of Engineering, Qassim University, Buraidah 51452, Saudi Arabia;
2. Metallurgical and Materials Engineering Department, Faculty of Petroleum and Mining Engineering, Suez University, Suez, Egypt;
3. Engineering Management Department, College of Engineering, Prince Sultan University, Riyadh, Saudi Arabia;
4. Center of Excellence for Research in Engineering Materials, King Saud University, Riyadh, Saudi Arabia

Received 4 March 2020; accepted 29 November 2020

Abstract: The effect of incorporating limited-diffusivity elements such as Fe and Ti on thermal stability of the nanocrystalline Al alloy was investigated. Al−10wt.%Fe and Al−10wt.%Fe−5wt.%Ti alloys were fabricated. The initial mixtures of powders were milled for 100 h in vacuum. The bulk samples were fabricated from the milled powders in a high frequency induction heat sintering (HFIHS) system. The milled powders and the bulk sintered samples were characterized by X-ray diffraction (XRD), Vickers microhardness, field emission scanning electron microscopy (FESEM-EDS) and transmission electron microscopy (TEM). The observations indicated that Fe and Ti were completely dispersed in the matrix to form a supersaturated solid solution (SSSS) with Al. Additionally, the inclusion of alloying elements led to an increase in hardness and yield strength of the alloy by 127% and 152%, respectively. The elevated temperature compression tests were carried out to evaluate the thermal stability of the alloys. The Al−10wt.%Fe−5wt.%Ti alloy revealed the optimum thermally stable behavior of the three alloys studied. The incorporation of Fe and Ti improved the thermal stability of the developed alloys through inhibiting the grain growth, hindering dissolution and growth of second phases (such as $Al_{13}Fe_4$ and $Al_{13}Ti$), and forming a stable solid solution.
Key words: nanocrystalline Al−Fe−Ti alloy; mechanical alloying; induction heat sintering; thermal stability; microstructure; mechanical properties

1 Introduction

Al alloys are being widely used in several applications due to their characteristic mechanical properties at room temperature. In addition, the characteristic specific strength makes them ideal for use in aerospace and automotive industry [1]. However, the current industrial use of Al and its alloys is limited to structures that operate at room or low temperatures, as they tend to lose their strength at elevated temperatures. In some cases, the strength deteriorates non-linearly with temperature [2]. The decrease in strength of the alloy can be attributed to the microstructural instability caused because of the substantial grain coarsening at high temperatures [3].

Based on the Hall−Petch [4,5] relationship, it is known that the average grain size of the alloy significantly influences its mechanical strength. The decrease in the grain size of an alloy to nanometer range has shown to improve its strength by several folds in comparison to its coarse-grained counterpart [6]. However, the nanocrystalline pure Al is found to be vulnerable when subjected to extremely high temperatures, mainly due to their microstructural instability. The microstructural instability in nanocrystalline Al arises due to the

Corresponding author: Hany Rizk AMMAR; Tel: +966-563309153; Fax: +966-163801152; E-mail: hanyammar@qec.edu.sa
DOI: 10.1016/S1003-6326(20)65475-9

substantial increase in the total free energy provided by the grain boundaries. In order to reduce the available free energy, there exists a large driving force that tends to increase the grain growth mechanism thereby reducing the grain boundary area of the nanocrystalline materials [7].

The grain growth mechanisms in nano-crystalline materials at elevated temperatures can be significantly restrained by the kinetic and thermodynamic stabilizations [7−9]. The kinetic stabilization is attained by decreasing the movement of the grain boundaries through the solute drag mechanism and Zener pinning by second phase particles. Being a thermally active mechanism, the kinetic stabilization is effective in controlling the grain growth in a low to moderate temperature regime [7]. However, at elevated temperatures the grain boundary pinning force will not be sufficient enough to impede the grain growth process. On the contrary, in thermodynamic stabilization the decrease in the grain boundary energy is achieved by the addition of solute atoms that tends to segregate at the grain boundaries [9,10].

The room temperature strength of wrought Al alloys is found to be ~600 MPa [11]. However, it is observed that the strength of Al alloys decreases non-linearly with an increase in temperature. Thus, the thermal and mechanical properties of Al alloys need to be further investigated in light of its thermal stability. There exist several methods to increase the high temperature strength of Al alloys. Some of the prominent ways that are frequently used including the selective incorporation of transition metals (TMs), alternate manufacturing processes and grain refinement.

The improved strength of Al−transition metal (TM) alloy at high temperatures is due to the development of supersaturated solid solution (SSSS) and hard intermetallics (secondary phases). The formation of SSSS and the precipitation of intermetallics are believed to enhance the microstructural stability to the alloy. Relatively, few investigations have been presented earlier to characterize the metallic powders that incorporate TMs as alloying elements [7,12−19]. A few investigations showed an improvement in the hardness of the alloys, while the others dealt with grain size stabilization and formation of intermetallic phases. Additionally, few investigations were based on the amount of alloying element present in the nanocrystalline alloy [18,20,21] and observed that the base alloy strength increased with an increase in the alloying element content. Thus, to fabricate Al alloys with improved strength, it is highly recommended to increase the concentration of the alloying element (TM). On the other hand, the solubility limit of TMs in pure metals is limited to 0.03%, even at elevated temperatures [22].

An improvement in manufacturing processes may also lead to the production of high strength Al alloys. In addition to introducing an improvement in manufacturing processes, several investigations were performed to explore different manufacturing processes that tend to enhance the solubility limit of TM. These processes include chemical vapor deposition (CVD) [23−25] for thin films, rapid solidification (RS) [26,27] and mechanical alloying (MA) [13,28−31]. All these processes received a significant importance as they all tend to increase the solubility of alloying elements. Of all these processes, MA is a widely used process because it leads to the grain refinement with increasing the limit of solid solubility.

In the current study, the effect of transition metals addition on the thermal stability of the developed nanocrystalline (NC) alloys was further investigated.

2 Experimental

2.1 Alloy synthesis

The starting powder and the mixture used in the present study include 99.9 wt.% pure Al, 90wt.%Al−10wt.%Fe and 85wt.%Al−10wt.%Fe−5wt.%Ti. The initial mixtures were degassed in vacuum while maintaining the degassing temperature at 373 K for 24 h. The degassed powders were transferred separately into the milling containers containing the required number of steel balls, so as to maintain a ball-to-powder mass ratio (BPR) of 10:1. The speed of milling was fixed to 120 r/min for 100 h. This speed is considered to be low enough to avoid heating of powders during milling. However, milling to long hours even at low speeds might increase the powder temperature. To address this issue, each milling cycle in the current investigation includes 15 min of milling followed by 15 min of holding time. During the MA process,

the powder particles undergo through heavy straining due to welding, fracturing and re-welding process [32]. These processes could lead to the adhesion of the fine particles. Various process control agents (PCA) have been used in earlier investigations which depend on the type of metallic powders being milled, the time of milling and the initial particle size of the powders [6,33−35]. The addition of stearic acid (PCA) with a content of 1 wt.% was used in the current study to avoid agglomeration of powder particles. The processed powders were transferred into the graphite dies in a controlled atmosphere and were sintered in a high frequency induction heat sintering (HFIHS) system under vacuum. The sintering was performed with a heating rate of 823 K/min up to 823 K and held at that temperature for 6 min under a pressing pressure of 50 MPa. Additionally, the densities of the bulk NC pure Al and alloys were determined using the Sartorius density measurement kit. The measured densities of the sintered NC pure Al, 90wt.%Al−10wt.%Fe and 85wt.%Al−10wt.%Fe−5wt.%Ti alloys were 2.685, 2.886 and 2.962, respectively.

2.2 Mechanical testing

The Vickers microhardness experiments were conducted on the NC alloys by means of Buehler hardness tester. The samples for hardness tests were finely ground and later polished using the standard procedures as described in the sample preparation techniques for microstructural measurements. The final polishing was achieved using colloidal silica suspension with particle size of 0.1 μm and an emery cloth. Several hardness measurements were recorded along the diameter of each sample with 0.25 mm spacing between each measurement.

To further investigate the effect of alloying elements on the strength and thermal stability of the produced alloys, the sintered samples were compression tested at a fixed strain-rate of 10^{-2} s^{-1}. The experimental temperatures were 623, 673, 723, 773, 823 and 873 K. The compression platens were lubricated with a high temperature grease to minimize the friction between the sample surfaces and the compression platens. The displacement obtained from the machine transducer was corrected for machine compliance. The corrected displacement values were used to determine the strains and the load from the machine transducer was used to calculate the stress.

2.3 Microstructure examination

The XRD analysis on the alloys fabricated in this study was performed on a Discover D8 diffractometer with a Cu K_α (λ=0.154 nm) radiation. The sample preparation for the XRD analysis including polishing of the sample surface was done in the case of hardness measurements. To produce a mirror finish sample surface, the polishing was achieved using colloidal silica suspension with particle size of 0.1 μm and an emery cloth. The standard silicon sample was used for correcting the instrument broadening and the peak width $\beta_{corr}(2\theta)$ was computed using the following equation [36]:

$$\beta^2_{corr}=\beta^2_{sample}-\beta^2_{std} \quad (1)$$

where the measured peak width of the sample is represented by β_{sample} and the standard sample peak width by β_{std}.

The XRD scanning rate was 0.2° per minute for a total 2θ range of 20°−80°. The 2θ scanning range selected in this study was adequate to capture the majority of the high intensity peaks of Al. From the XRD peak profiles data, it is known that the low angle peak reflects the grain size and the high angle peak reflects the accumulated strain [37]. With this understanding, the peak corresponding to the (111) plane of Al was considered in calculating the average crystallite size through the Debye−Scherrer's equation [38] given as

$$D=\frac{K\lambda}{B\cos\theta} \quad (2)$$

where the crystallite size is represented by D, constant K is the shape factor (assumed as 0.9), λ is the wavelength (0.154 nm) of Cu K_α radiation, θ represents the Bragg angle and B represents the width (full width at half maximum, in radian) of the peak.

The lattice parameter (a), was calculated using the Bragg's law [39] given by

$$2d_{hkl}\sin\theta=n\lambda \quad (3)$$

where n is an integer, the inter-planar spacing is represented by d_{hkl}, λ is the wavelength of the incident wave. Using the crystallographic planes and the Bragg's law, the lattice parameter (a), for the crystal can be calculated using the following relationship:

$$d_{hkl}=\frac{a}{\sqrt{h^2+k^2+l^2}} \quad (4)$$

FESEM equipped with an energy dispersive X-ray (EDX) analyzer and HRTEM were used to characterize the initial and milled (MA processed) powders. The TEM powder samples were prepared through the sonication process.

3 Results and discussion

3.1 Microstructure characteristics of starting and MA powders

The morphologies of as-received pure Al, Fe and Ti powders along with 100 h milled mixture (powder) are shown in Fig. 1. The as-received (initial) Al powder used for milling was observed to be spherical (particle size of 3 μm) as shown in Fig. 1(a). The average particle sizes of the pure Fe and Ti powders were 45 μm with a spherical morphology. In order to reduce the difference between the initial particle size of the Al powder and the Fe and Ti powders, the later powders were ball milled for 6 h under argon atmosphere. After milling, the average sizes of the Ti and Fe powders particles diminish to 8 and 5 μm, respectively. However, the morphology of the milled powder transformed from near spherical shape (initially) to flake-shape, as may be noticed in Figs. 1(c) and (e). Subsequently, a close observation of Fig. 1(d)

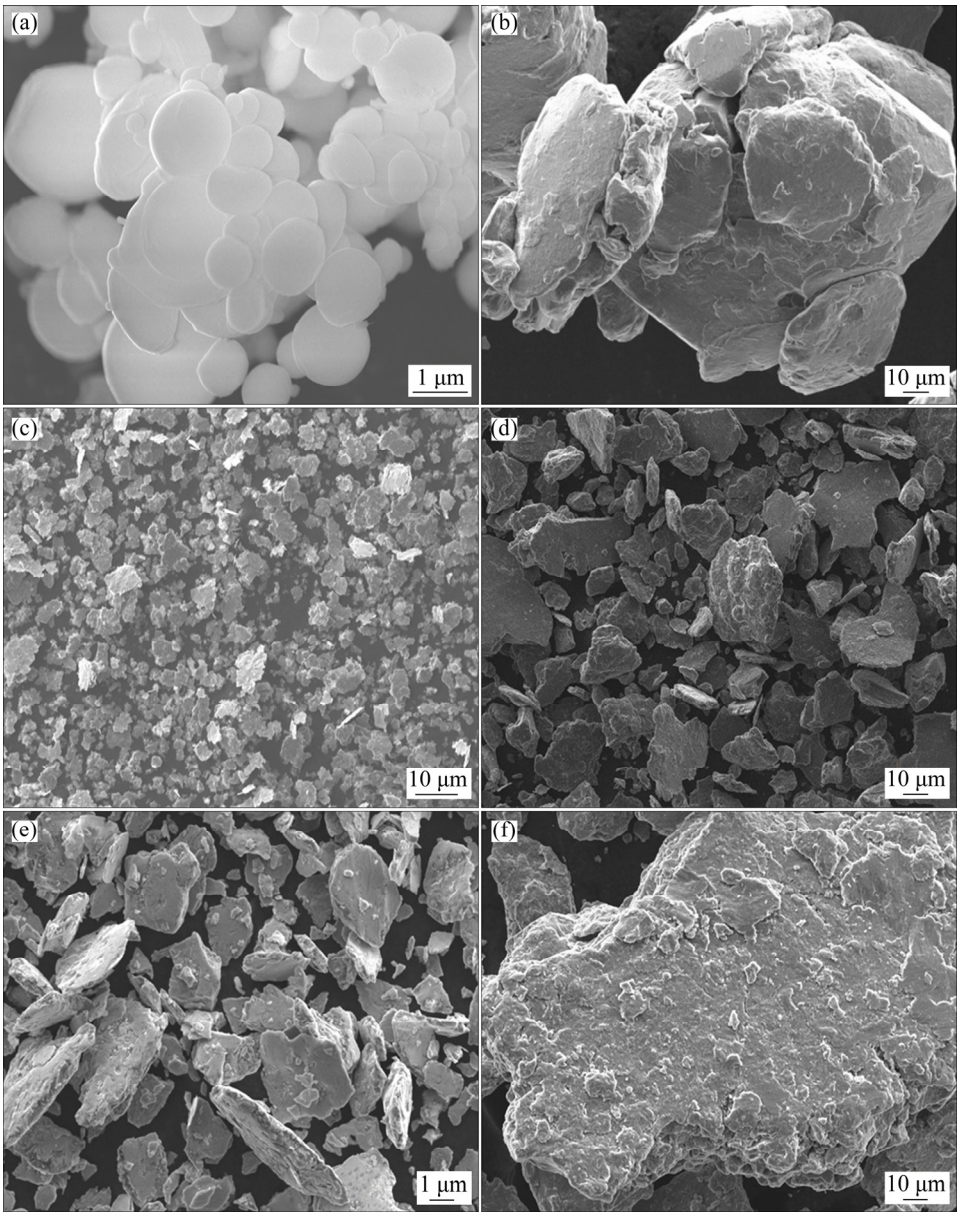

Fig. 1 Secondary electron images of powders: (a) Pure Al; (b) As-milled Al; (c) Pure Fe; (d) As-milled Al−10wt.%Fe powder for 100 h; (e) Pure Ti; (f) As-milled Al−10wt.%Fe−5wt.%Ti powder for 100 h

indicates that the alloyed mixture (after 100 h) was also flaked. Figure 1(f) shows the morphology of the Al−10wt%.Fe−5wt.%Ti alloy powders milled for 100 h. From the morphology of the processed alloys it is clear that the amount of PCA used (1 wt.%) in the current investigation was not sufficient to prevent or minimize the powder agglomeration.

Figures 2(a−c) display the XRD patterns of the alloys in as-mixed, milled and sintered conditions for Al, Al−10wt.%Fe and Al−10wt.%Fe−5wt.%Ti, respectively. From Fig. 2, it is noted that the diffraction peaks of milled and sintered samples were shifted to high angles. The observed 2θ peak shifts of the examined alloys after milling are shown in Tables 1, 2 and 3, respectively. The shifting of peak position of the milled powder indicates the diffusion of Fe and Ti particles into the Al matrix. The absence of Fe peak in the milled powders (after MA) of the two alloys could be attributed to the overlapping of Al peak with that of Fe peak. In addition, the broadening and shortening (decreased intensity) of peaks were observed in the milled and sintered samples, indicating the reduction in the crystallite size of the alloys studied. To further confirm the presence of Fe and Ti elements in the matrix of the alloy (after MA), the EDX analysis was achieved on the milled powder.

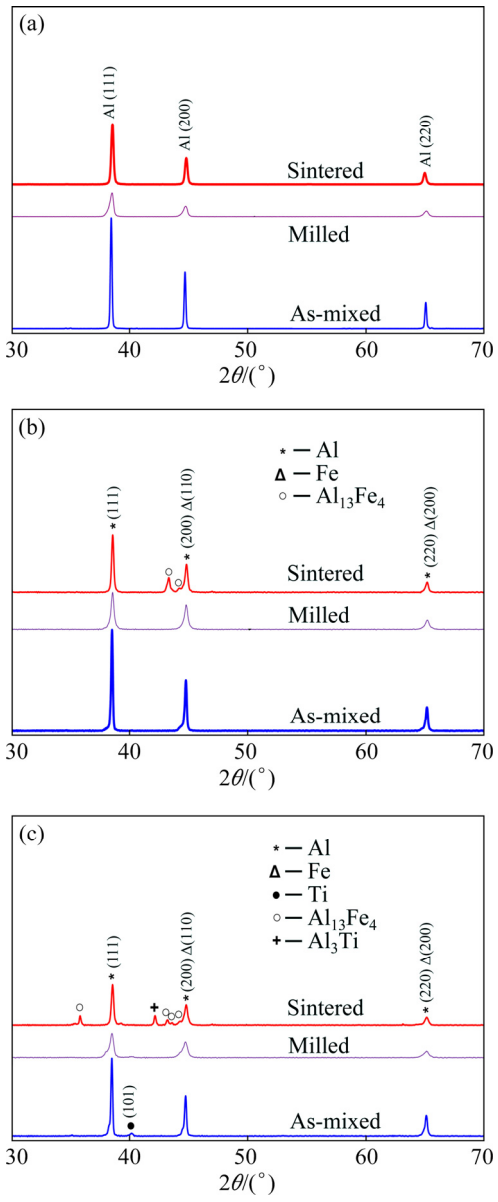

Fig. 2 XRD patterns of as-mixed, milled powders for 100 h and sintered sample: (a) Al; (b) Al−10wt.%Fe; (c) Al−10wt.%Fe−5wt.%Ti

Table 1 XRD peak position for pure Al

Condition	2θ/(°)		
	Peak 1	Peak 2	Peak 3
As-mixed	38.4308	44.6887	65.0654
Milled	38.4322	44.7115	65.0989
Sintered	38.4387	44.718	65.1054

Table 2 XRD peak position for Al−10wt.%Fe alloy

Condition	2θ/(°)		
	Peak 1	Peak 2	Peak 3
As-mixed	37.9715	44.7197	65.1071
Milled	38.2111	44.7789	65.1867
Sintered	38.2373	44.8062	65.2128

Table 3 XRD peak position for Al−10wt.%Fe−5wt.%Ti alloy

Condition	2θ/(°)		
	Peak 1	Peak 2	Peak 3
As-mixed	38.5016	44.7401	65.1275
Milled	38.5388	44.7978	65.2084
Sintered	38.5637	44.8205	65.2656

The results obtained from the EDX for Al−10wt.%Fe and Al−10wt.%Fe−5wt.%Ti alloys are shown in Figs. 3(a′) and (b′), respectively. The EDX analysis clearly displayed the existence of Fe and Ti in the milled powders. In addition, the elemental composition from the EDX analysis of the sintered alloys revealed the existence of alloying elements within ±2 wt.% of the initial mixture

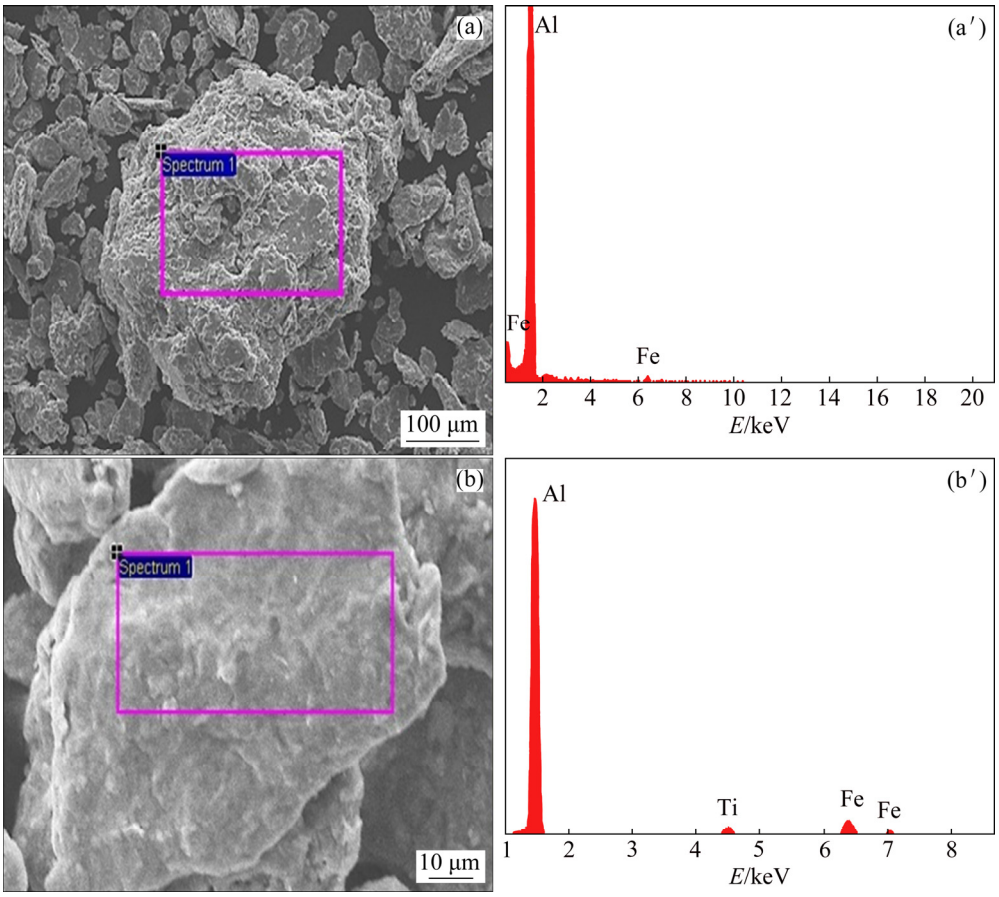

Fig. 3 Secondary electron micrographs (a, b) and corresponding chemical composition using EDX (a′, b′) for 100 h milled powders: (a, a′) Al−10wt.%Fe; (b, b′) Al−10wt.%Fe−5wt.%Ti

composition before milling. Thus, it could be interpreted that the mechanical alloying of 10 wt.% Fe and 10wt.%Fe−5wt.%Ti with Al resulted in the complete dissolution of Fe and Ti in Al matrix.

Figure 4 shows the difference in the crystallite size from milled powder to sintered bulk pure Al, Al−10wt.%Fe and Al−10wt.%Fe−5wt.%Ti alloy. The size of crystal was calculated using the Debye−Scherrer's equation. From the figure, it is observed that the sintering conditions used in the current study were effective in producing bulk sample without significant increase in the crystallite size. The maximum intensity peak was used to calculate the crystallite size based on the fact that the lower diffraction angle peak influences the crystallite size of the sample. The results indicate that the maximum difference in the crystallite size of 4 nm was observed in Al−Fe−Ti alloy.

Table 4 lists the variations in the lattice parameter of the processed alloys in different conditions. The maximum value of lattice parameter was observed in the as-mixed condition

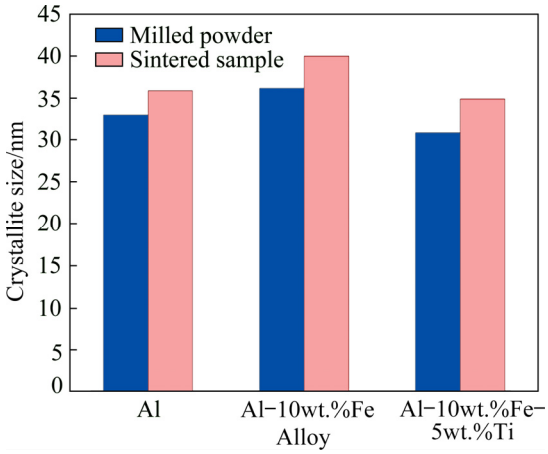

Fig. 4 Difference in crystallite size from milled powder to sintered bulk samples

irrespective of the processing conditions. The lowest value of lattice parameter was observed in the sintered sample for a given alloy. In the case of pure Al, the variation in the lattice parameter was observed to be minimal. This observation was as expected due to the absence of additional alloying elements in pure Al. However, in the case of other

Table 4 Difference in lattice parameter of processed alloys

Material	Condition	Lattice parameter/nm
Al	As-mixed	0.4054
	Milled	0.4054
	Sintered	0.4053
Al−10wt.%Fe	As-mixed	0.4101
	Milled	0.4076
	Sintered	0.4074
Al−10wt.%Fe−5wt.%Ti	As-mixed	0.4047
	Milled	0.4043
	Sintered	0.4041

two alloys, the lattice parameter was observed to decrease from the as-mixed to sintered condition. Based on the experimental results, the dissolution of alloying elements can be attributed to the decrease in the lattice parameter of the consolidated alloy. This observation agrees with the results displayed in Fig. 3.

To further confirm the presence of alloying element in Al−10wt.%Fe alloy, SEM elemental mapping was performed on the alloy. Figure 5(a) shows the mapping of heat-treated milled powders subjected to the same temperature and time of the sintering process. Similarly, Fig. 5(b) shows the EDS elemental mapping of the sintered samples. Based on the results shown in Fig. 5, it is clearly established that the MA process adopted in the current study has led to the homogeneous distribution of the alloying elements in the base matrix.

Similarly, SEM elemental mapping was performed on Al−10wt.%Fe−5wt.%Ti alloy to confirm the existence of alloying additions in the bulk alloy. The results from the EDX are shown in Fig. 6. Based on the results of the heat-treated milled powders which subjected to the same temperature and time of sintering process (Fig. 6(a) and bulk sample shown in Fig. 6(b)), it is clearly established that the alloying process adopted in the current study has resulted in uniform distribution of

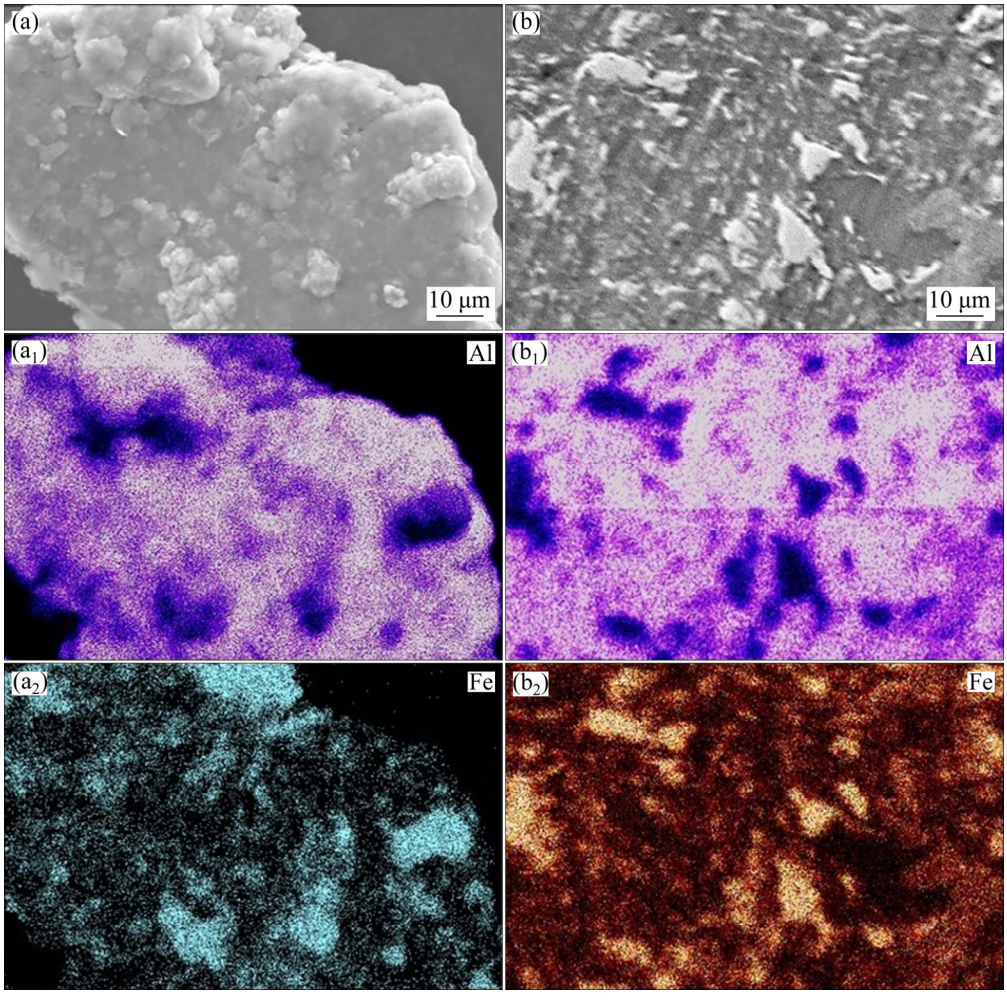

Fig. 5 SEM mapping of Al−10wt.%Fe alloy: (a, a_1, a_2) Heat-treated milled powders; (b, b_1, b_2) Sintered sample

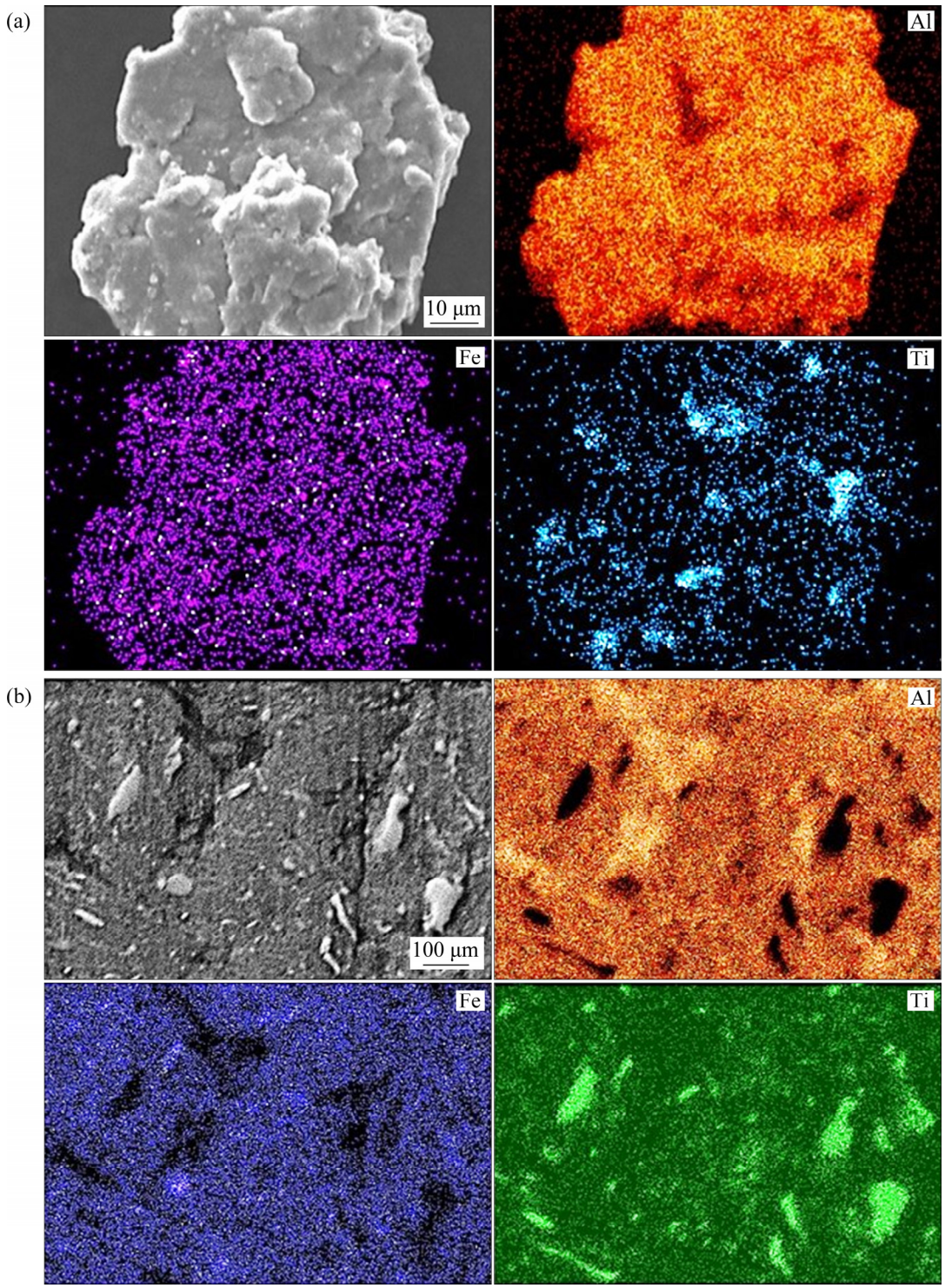

Fig. 6 SEM mapping of Al−10wt.%Fe−5wt.%Ti alloy: (a) Heat-treated milled powders; (b) Sintered sample

alloying elements (Fe and Ti) in Al matrix. The dispersion of alloying elements was in the form of supersaturated solid solution with Al matrix. However, with further sintering the alloying elements formed precipitates or intermetallic that led to the enhancement in the observed mechanical properties of the sintered alloys.

The XRD analysis on the milled powders did not reveal the presence of alloying elements (Fe and Ti). This may be attributed to the overlapping of the diffraction peaks of processed elements. On the contrary, the EDS of the milled powder indicated the presence of the TMs (Fe and Ti). This could mean that the TMs formed the super saturated

solutions with Al matrix. The super saturated solutions were metastable and led to the formation of second phases during the sintering heating cycle. The XRD results on the sintered alloys showed the evolution of $Al_{13}Fe_4$ and Al_3Ti secondary phases.

Figure 7 displays the HRTEM micrographs of the bulk samples. The heat-treated milled powder for TEM analysis was obtained by sintering process without the application of pressure. The presence of sharp rings on the SAED pattern clearly indicates that the alloy shows a high degree of crystallinity. The average crystallite sizes measured using TEM were found to be 30 and 25 nm for Al−10wt.%Fe and Al−10wt.%Fe−5wt.%Ti alloys, respectively. The results were in a good agreement with the obtained results from applying the Scherer's equation (see Fig. 4).

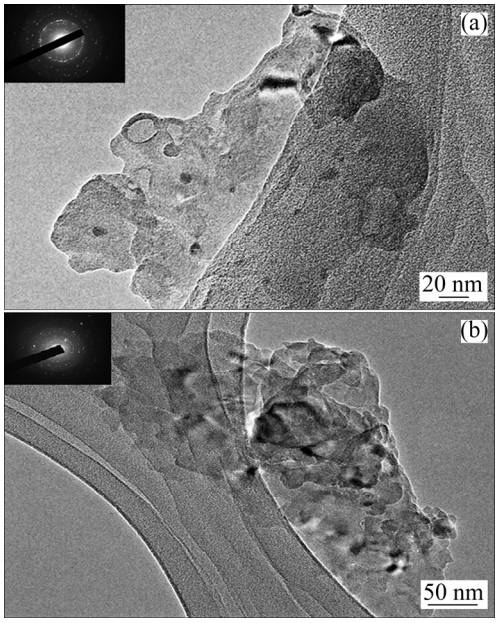

Fig. 7 HRTEM micrographs of heat-treated milled powders along with SAD pattern (insert): (a) Al−10wt.%Fe; (b) Al−10wt.%Fe−5wt.%Ti

3.2 Hardness and compressive strength of bulk samples

The distribution of the hardness values on the studied samples is shown in Fig. 8. The hardness measurements were performed on one of the sample faces. The indents were taken at every 0.25 mm along the diameter of the cylindrical surface. From the figure, it is clear that the addition of TM has resulted in improving the hardness of the alloy. Also, it is observed that the hardness profile of Al−10wt.%Fe and Al−10wt.%Fe−5wt.%Ti alloy is similar to that of pure Al. This observation implies that MA leads to the homogeneous diffusion of the alloying elements in Al matrix. The maximum value of hardness (2.5 GPa) was attained in Al−10wt.%Fe−5wt.%Ti alloy. While the hardnesses of pure Al (milled for 100 h) and Al−10wt.%Fe alloy were found to be 1.15 and 1.75 GPa, respectively. When compared to the pure Al (milled), the percentage increase in the hardness of Al−10wt.%Fe−5wt.%Ti alloy is found to be 117%. This implies that the addition of TM has enhanced the hardness of the developed alloy. Similarly, when compared to the hardness of coarse-grained Al (without milling), the hardness of the milled alloy is improved by 635%.

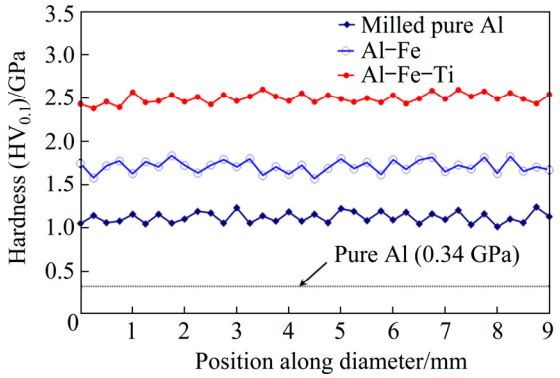

Fig. 8 Hardness profile of sintered alloy

To demonstrate the improvement in the thermal stability of the studied alloys, high temperature compressive experiments were carried out on the processed alloys at a fixed strain rate (10^{-2} s^{-1}) and the temperature range is 623−873 K. The compressive experimental responses of pure Al (milled for 100 h) at different temperatures are shown in Fig. 9. A nonlinear drop in the yield strength of pure Al sample was observed. This response (nonlinear drop) was similar to that of coarse-grained pure Al with an exception of lower strength when compared with pure Al obtained from milled (fine-grained) powders. The failure strain was observed to augment with rising temperature up to 723 K.

Figure 10 reveals the difference in the yield strength of the processed samples with test temperature. The yield strength values reported in this figure represents the 0.2% offset yield strength. It is observed that the alloy strength lessened non-linearly with rising temperature. The yield strength of pure aluminum was noted to be 155 MPa at 723 K, whereas the yield strength of Al−10wt.%Fe−5wt.%Ti alloy is found to be 390 MPa at 723 K

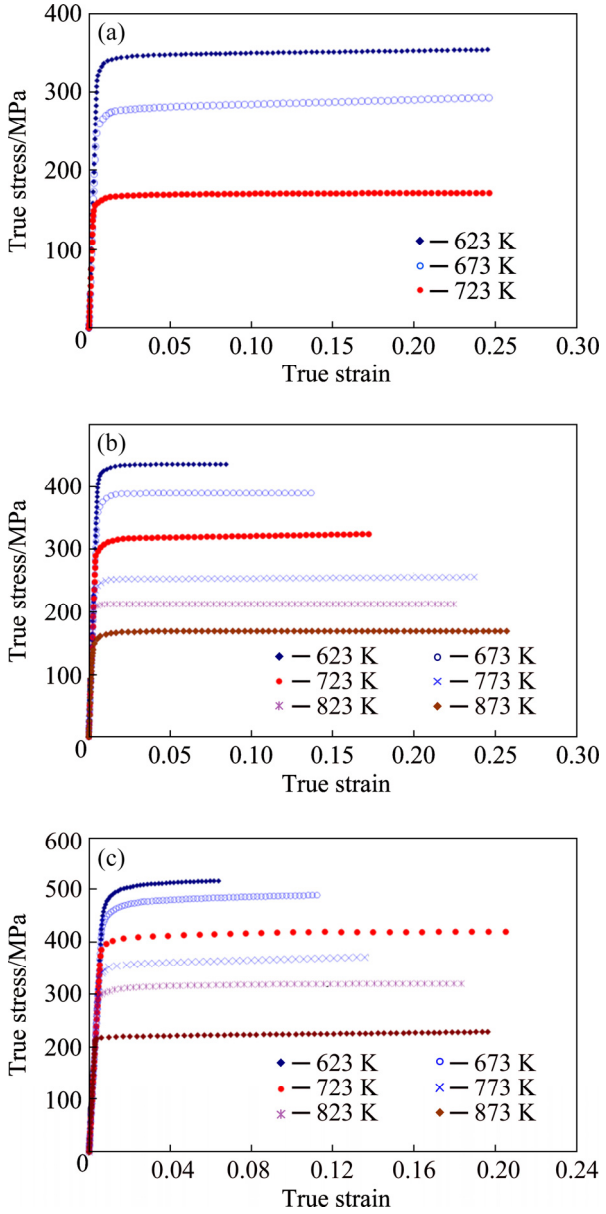

Fig. 9 Compressive stress−strain curves of bulk alloys at various temperatures and performed at strain rate of 10^{-2} s^{-1}: (a) Al; (b) Al−10wt.%Fe; (c) Al−10wt.%Fe−5wt.%Ti

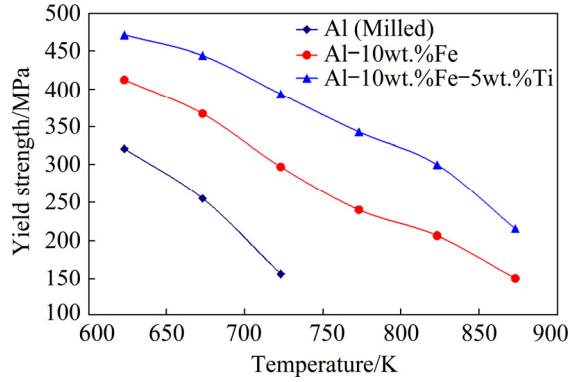

Fig. 10 Difference in yield strength of sintered alloys at different temperatures

(an increase of more than 2 folds when compared with pure Al) and 220 MPa at 875 K. This demonstrates that the alloys produced in this study showed an increase in the strength of the alloys at higher temperatures and can be inferred as an increase in thermal stability in the developed alloys.

The compression experiments applied on the bulk samples at various temperatures indicate the non-linear deviation of the yield strength with an increase in temperature. Additionally, it was noticed that the presence of alloying elements and more often due to the occurrence of secondary phases in the microstructure, the alloys showed significant strength retention at higher temperatures when compared to the strength of pure Al at these temperatures. Thus, the Al alloys produced in this study exhibited a notable increase in their thermal stability.

It is well known that the nanocrystalline materials show acceptable mechanical properties at high temperatures. The instability of the microstructure at high temperature is attributed to the softening mechanisms such as grain coarsening and second phase precipitates growth and dissolution. In the present study, the microstructural thermal stability of Al alloys was improved by the addition of Fe and Ti as alloying elements. These elements display low diffusivity in Al matrix and consequently activation energy is required to allow the diffusion of Fe and Ti in Al. The solid solution and second phases containing Fe and Ti will remain stable even with increasing the temperature to specific values due to the low diffusivity of Fe and Ti in Al. Accordingly, the thermal stability revealed in the present study was attributed to the presence of such low diffusivity elements which resist the grain growth and dissolution of second phases such as $Al_{13}Fe_4$ and Al_3Ti. The experimental investigation through XRD, EDX and TEM techniques has shown that the successful alloying of Fe and Ti with Al was achieved. The use of the optimized combination of temperature and pressure in the sintering process has resulted in precipitation of the secondary phases without significant grain coarsening. This is clearly evident from the XRD peaks which indicate the dissolution of alloying elements in the milled powder and precipitation of the intermetallics during the sintering process, without significant change in the width of the peaks when compared to the peaks of the milled power.

Based on the experimental results from the XRD, it can be inferred that the grain coarsening of the alloys was significantly reduced due to the presence of solute atoms (Fe and Ti) resulting in the thermodynamic stabilization and the precipitation of stable intermetallics provided the kinematic stabilization through the pinning of the grain boundaries of the alloy. These stabilizations improved the microstructural stability of the alloy. The increase in the hardness and the yield strength of the alloys when compared to the nanocrystalline pure Al at high temperatures clearly indicates the improvement in the thermal stability of the alloys with Fe and Ti additions. The high strength revealed by the alloy in the compression experiments at high temperatures establishes that the solute atoms and the precipitates provided the limited grain growth to achieve the stable microstructures at high temperatures and thereby resulting in the improvement in the thermal stability of the processed alloys.

4 Conclusions

(1) The MA process of the initial coarse grained mixture has successfully produced nanocrystalline Al−10wt.%Fe−5wt.%Ti alloys in the powder form, as a SSSS of iron (Fe) and titanium (Ti) in aluminum (Al) matrix.

(2) The precipitation of intermetallic or secondary phase particles from the nanocrystalline Al−10wt.%Fe and Al−10wt.%Fe−5wt.%Ti alloys, was initiated during sintering process.

(3) The precipitation of metastable, Al_6Fe and the stable $Al_{13}Fe_4$ and Al_3Ti intermetallic or secondary phases in the sintered alloys, was observed through the XRD technique.

(4) Compared to the yield strength of nanocrystalline Al alloy at 723 K, the addition of Fe and Fe+Ti in Al matrix has resulted in increasing the yield strength by 90% and 152%, respectively.

(5) The Fe and Fe+Ti additions have resulted in an increase in an average hardness by 45% and 127%, respectively when compared to the average hardness of the nanostructured Al.

(6) The addition of limited-diffusivity elements of Fe and Ti revealed an effective role in improving the thermal stability of the alloys studied through inhibiting the grain growth, hindering dissolution and growth of second phases (such as $Al_{13}Fe_4$ and $Al_{13}Ti$), and forming a stable solid solution.

References

[1] BAIG M, KHAN A S, CHOI S H, LEE E. Effect of manufacturing processes and welding type on quasi-static and dynamic responses of aluminum alloys: Experiments and modeling [J]. Journal of Dynamic Behavior of Materials, 2015, 1: 299−314.

[2] KHAN A S, BAIG M. Anisotropic responses, constitutive modeling and the effects of strain-rate and temperature on the formability of an aluminum alloy [J]. International Journal of Plasticity, 2011, 27: 522−538.

[3] DEVARAJ A, WANG W, VEMURI R, KOVARIK L, JIANG X, BOWDEN M, TRELEWICZ JR, MATHAUDHU S, ROHATGI A. Grain boundary segregation and intermetallic precipitation in coarsening resistant nanocrystalline aluminum alloys [J]. Acta Materialia, 2019, 165: 698−708.

[4] HALL E. The deformation and ageing of mild steel: III Discussion of results [J]. Proceedings of the Physical Society Section B, 1951, 64: 747−753.

[5] PETCH N. The cleavage strength of polycrystals [J]. J Iron Steel Inst, 1953, 174: 25−28.

[6] KHAN A S, FARROKH B, TAKACS L. Effect of grain refinement on mechanical properties of ball-milled bulk aluminum [J]. Materials Science and Engineering A, 2008, 489: 77−84.

[7] SABER M, KOTAN H, KOCH C C, SCATTERGOOD R O. Thermal stability of nanocrystalline Fe−Cr alloys with Zr additions [J]. Materials Science and Engineering A, 2012, 556: 664−670.

[8] LIU F, KIRCHHEIM R. Comparison between kinetic and thermodynamic effects on grain growth [J]. Thin Solid Films, 2004, 466: 108−113.

[9] DOR A, CHRISTOPHER A S. Interplay between thermodynamic and kinetic stabilization mechanisms in nanocrystalline Fe−Mg alloys [J]. Acta Materialia, 2018, 144: 447−458.

[10] ROY D, MAHESH B, ATWATER M, CHAN T, SCATTERGOOD R, KOCH C. Grain size stability and hardness in nanocrystalline Cu−Al−Zr and Cu−Al−Y alloys [J]. Materials Science and Engineering A, 2014, 598: 217−223.

[11] POLMEAR I. Light alloys [M]. 4th ed. Oxford: Butterworth-Heinemann Elsevier Ltd., 2005.

[12] LIANG J, KONG C, QUADIR M, ZHENG Y, YAO X, MUNROE P. Microstructure and mechanical properties of a bulk ultrafine grained Al−7Si−0.3Mg alloy produced by thermomechanical consolidation of a nanocrystalline powder [J]. Materials Science and Engineering A, 2016, 658: 192−202.

[13] BAIG M, AMMAR H R, SEIKH A H. Thermo-mechanical responses of nanocrystalline Al−Fe alloy processed using mechanical alloying and high frequency heat induction

sintering [J]. Materials Science and Engineering A, 2016, 655: 132−141.

[14] LI L, SABER M, XU W, ZHU Y, KOCH C C, SCATTERGOOD R O. High-temperature grain size stabilization of nanocrystalline Fe−Cr alloys with Hf additions [J]. Materials Science and Engineering A, 2014, 613: 289−295.

[15] DUBIEL S, COSTA B, CIESLAK J, BATISTA A. Debye temperature of nanocrystalline Fe−Cr alloys obtained by mechanical alloying [J]. Journal of Alloys and Compounds, 2015, 649: 1246−1252.

[16] SHI X, CHEN Y, MA X, WANG H, LIU F. Microstructural evolution of nanocrystalline Fe−Zr alloys upon annealing treatment [J]. Materials Characterization, 2015, 103: 58−64.

[17] KENNETH K A, MICHAEL O B, SAMUEL R O. Processing, alloy composition and phase transition effect on the mechanical and corrosion properties of high entropy alloys: a review [J]. Journal of Materials Research and Technology, 2016, 5(4): 384−393.

[18] NAYAK S, WOLLGARTEN M, BANHART J, PABI S, MURTY B. Nanocomposites and an extremely hard nanocrystalline intermetallic of Al−Fe alloys prepared by mechanical alloying [J]. Materials Science and Engineering A, 2010, 527: 2370−2378.

[19] SASAKI T, MUKAI T, HONO K. A high-strength bulk nanocrystalline Al−Fe alloy processed by mechanical alloying and spark plasma sintering [J]. Scripta Materialia, 2007, 57: 189−192.

[20] FILIP P, DALIBOR V, MARKÉTA B, ALENA M, TOMÁŠ F K, JAKUB Č. Structure and mechanical properties of Al−Si−Fe alloys prepared by short-term mechanical alloying and spark plasma sintering [J]. Materials & Design, 2015, 75: 65−75.

[21] MENDIS C, JHAWAR H, SASAKI T, OH-ISHI K, SIVAPRASAD K, FLEURY E, HONO K. Mechanical properties and microstructures of Al−1Fe−(0−1)Zr bulk nano-crystalline alloy processed by mechanical alloying and spark plasma sintering [J]. Materials Science and Engineering A, 2012, 541: 152−158.

[22] KATTNER U, MASSALSKI T B. Binary alloy phase diagrams [M]. Material Park, OH: ASM International, 1990: 148.

[23] LOUKYA B, NEGI D, SAHU R, PACHAURI N, GUPTA A, DATTA R. Structural characterization of epitaxial $LiFe_5O_8$ thin films grown by chemical vapor deposition [J]. Journal of Alloys and Compounds, 2016, 668: 187−193.

[24] STOCK H R, KÖHLER B, BOMAS H, ZOCH H W. Characteristics of aluminium–scandium alloy thin sheets obtained by physical vapour deposition [J]. Materials & Design, 2010, 31: 76−81.

[25] POPOVSKA N, GERHARD H, WURM D, POSCHER S, EMIG G, SINGER R. Chemical vapor deposition of titanium nitride on carbon fibres as a protective layer in metal matrix composites [J]. Materials & Design, 1997, 18: 239−242.

[26] LUCCHETTA M C, SAPORITI F, AUDEBERT F. Improvement of surface properties of an Al−Sn−Cu plain bearing alloy produced by rapid solidification [J]. Journal of Alloys and Compounds, 2019, 805: 709−717.

[27] YAOJUN L, SHUAIYING M, ZHIGANG Y, YAQI Z, LIMIN W. The enhanced microhardness in a rapidly solidified Al alloy [J]. Materials Science and Engineering A, 2017, 692: 182−191.

[28] AGUILAR C, GUZMAN P, LASCANO S, PARRA C, BEJAR L, MEDINA A. Solid solution and amorphous phase in Ti−Nb−Ta−Mn systems synthesized by mechanical alloying [J]. Journal of Alloys and Compounds, 2016, 670: 346−355.

[29] AL-JOUBORI A A, SURYANARAYANA C. Synthesis of metastable $NiGe_2$ by mechanical alloying [J]. Materials & Design, 2015, 87: 520−526.

[30] MAULIK O, KUMAR V. Synthesis of $AlFeCuCrMg_x$ (x=0, 0.5, 1, 1.7) alloy powders by mechanical alloying [J]. Materials Characterization, 2015, 110: 116−125.

[31] MASMOUDI M, MHADHBI M, ESCODA L, SUÑOL J, KHITOUNI M. Microstructural evolution and corrosion behavior of nanocrystalline FeAl synthesized by mechanical alloying [J]. Journal of Alloys and Compounds, 2016, 657: 330−335.

[32] SURYANARAYANA C. Mechanical alloying and milling [J]. Progress in Materials Science, 2001, 46: 1−184.

[33] BAIG M, AMMAR H R, SEIKH A H, MOHAMMED J A, ALMUFADI F, ALABOODI A. Thermal stability of nanocrystalline Al−10Fe−5Cr bulk alloy [J]. Transactions of Nonferrous Metals Society of China, 2019, 29(2): 242−252.

[34] SURYANARAYANA C, FROES F. Nanocrystalline titanium-magnesium alloys through mechanical alloying [J]. Journal of Materials Research, 1990, 5: 1880−1886.

[35] WANG J S, DONNELLY S G, GODAVARTI P, KOCH C C. Microstructures and mechanical behavior of mechanically alloyed nickel aluminide [J]. International Journal of Powder Metallurgy, 1988, 24(4): 315−325.

[36] WARREN B E. X-ray diffraction [M]. New York: Addison-wesley, 1969.

[37] WILLIAMSON G, HALL W. X-ray line broadening from filed aluminium and wolfram [J]. Acta Metallurgica, 1953, 1: 22−31.

[38] PATTERSON A. The Scherrer formula for X-ray particle size determination [J]. Physical Review, 1939, 56: 978−981.

[39] BRAGG W H, BRAGG W L. The reflecion of X-rays by crystals [J]. Proceedings of the Royal Society A, 1913, 88(605): 428−38.

合金化元素对纳米晶铝合金热稳定性的影响

Hany Rizk AMMAR[1,2], Muneer BAIG[3], Asiful Hossain SEIKH[4], Jabair Ali MOHAMMED[4]

1. Mechanical Engineering Department, College of Engineering, Qassim University, Buraidah 51452, Saudi Arabia;
2. Metallurgical and Materials Engineering Department, Faculty of Petroleum and Mining Engineering, Suez University, Suez, Egypt;
3. Engineering Management Department, College of Engineering, Prince Sultan University, Riyadh, Saudi Arabia;
4. Center of Excellence for Research in Engineering Materials, King Saud University, Riyadh, Saudi Arabia

摘　要：为研究加入 Fe 和 Ti 扩散系数有限的元素对纳米晶铝合金热稳定性的影响，制备 Al−10%Fe(质量分数)和 Al−10%Fe−5%Ti(质量分数)合金。将初始混合粉末在真空下球磨 100 h，用高频感应加热烧结系统将球磨后的粉末制备成块体样品。采用 X 射线衍射仪、维氏显微硬度仪、场发射扫描电子显微镜和透射电子显微镜对球磨后的粉末和烧结后的块体样品进行表征。结果表明，Fe 和 Ti 完全分散在基体中，与 Al 形成过饱和固溶体。另外，合金元素的加入使合金的硬度和屈服强度分别提高 127%和 152%。通过高温压缩试验评估合金的热稳定性，结果显示 3 种合金样品中 Al−10%Fe−5%Ti 合金的热稳定性最好。Fe 和 Ti 的加入抑制合金的晶粒长大，阻碍第二相如 $Al_{13}Fe_4$ 和 $Al_{13}Ti$ 的分解、长大，形成稳定的固溶体，从而提高合金的热稳定性。

关键词：纳米晶 Al−Fe−Ti 合金；机械合金化；感应加热烧结；热稳定性；显微组织；力学性能

(Edited by Xiang-qun LI)